Oxidation of Ethyne and But-2-yne. 2. Master Equation Simulations

Andrea Maranzana,[†] John R. Barker,*[,†] and Glauco Tonachini[‡]

Department of Atmospheric, Oceanic, and Space Sciences, 1520 Space Research Building, 2455 Hayward Street, University of Michigan, Ann Arbor, Michigan, 48109-2143, and Dipartimento di Chimica Generale ed Organica Applicata, Università di Torino, Corso Massimo D'Azeglio 48, I-10125 Torino, Italy

Received: September 6, 2007; In Final Form: January 25, 2008

The aim of this study is to improve understanding of the tropospheric oxidation of ethyne (acetylene, C_2H_2) and but-2-yne, which takes place in the presence of HO and O_2. The details of the potential energy hypersurface have been discussed in a previous article [Maranzana et al., *J. Phys. Chem. A* **2008**, *112,* XXXX]. For both molecules, the initial addition of HO radical to the triple bond is followed by addition of O_2 to form peroxyl radicals. In both reaction systems, the peroxyl radicals take two isomeric forms, **E1** and **E2** for ethyne and **e1** and **e2** for but-2-yne. Energy transfer parameters ($\alpha = 250$ cm^{-1}) for the ethyne system were obtained by simulating laboratory data for N_2 buffer gas, where O_2 was not present. In simulations of C_2H_2 + HO when O_2 is present, **E1** reacts completely and **E2** reacts almost completely, before thermalization. Radical **E1** produces formic acid (∼44%) and **E2** gives glyoxal (∼53%), in quite good agreement with experiments. For but-2-yne, pressure-dependent laboratory data are too scarce to obtain energy transfer parameters directly, so simulations were carried out for a range of values: $\alpha = 200-900$ cm^{-1}. Excellent agreement with the available experimental yields at atmospheric pressure was obtained with $\alpha = 900$ cm^{-1}. Two reaction channels are responsible for acetic acid formation, but one is clearly dominant. Biacetyl is produced by reactions of **e1** and, to a minor extent, **e2**. The peroxyl radical **e2** leads to less than 8% of all products. Vinoxyl radical (which has been reported in experiments involving C_2H_2 + HO) and products of its reactions are predicted to be negligible under atmospheric conditions.

Introduction

Alkynes are released in earth's atmosphere by combustion processes.[1] They are important intermediates in combustion, particularly in soot formation. The principal atmospheric loss processes for the alkynes are their reactions with HO; the chemical lifetimes are estimated to be days to weeks.[1,2] With the longer lifetimes, substantial transport of the alkynes may take place horizontally over intercontinental distances and vertically to altitudes near the tropopause. A number of studies have been reported on the reaction rates of HO + C_2H_2 as a function of temperature, pressure and buffer gas.[2−10] Product distributions have also been reported for various experimental conditions.[11−20] Only limited information[14,19,21] is available for the but-2-yne system.

In the preceding paper[22] (paper 1) of this series, we reported the results of electronic structure calculations on the reaction systems initiated by the reactions of HO radical with ethyne (acetylene, C_2H_2) and with but-2-yne ($CH_3-C\equiv C-CH_3$) in the presence of O_2. The reaction schemes reported there generally support the experimental product distributions. In the present paper, we use the molecular properties and transition structures parameters calculated in paper 1 to construct master equation models for the two reaction systems. We include not only the unimolecular isomerization and fragmentation reactions stemming from the initial adduct formation but also potentially competitive bimolecular reactions with O_2 and subsequent reactions of the more highly oxidized species. This is accomplished by using the semi-microcanonical pseudo-first-order reaction approach described previously.[23] After minor adjustments of reaction barriers, the master equation models that result from this analysis give good quantitative agreement with recent measurements and are suitable for use in atmospheric chemistry simulations. With some modifications and extensions, they could also be used for simulations under combustion conditions.

In the following, we will first describe the reaction schemes arrived at in paper 1, followed by a section summarizing experimental rate and product studies on these reaction systems. We then describe the master equation methods, our results, and conclusions.

Reaction Mechanisms

The electronic structure calculations reported in the preceding paper[22] (paper 1) produced information about stationary points on the potential energy surfaces (PESs), which is needed for constructing master equation models. This information includes geometries of optimized structures, moments of inertia, vibrational frequencies, and relative potential energies of species and transition structures (TSs). For convenience, these data are summarized in this paper and the associated Supporting Information. As discussed in paper 1, the results are in generally good agreement with the parts of the PES previously studied by other researchers.

The reaction schemes for ethyne and but-2-yne are very similar, except that but-2-yne can undergo more reactions than ethyne. In both cases, the initial step is addition of HO radical to the triple bond to form an adduct, which has two isomeric forms (**B1** and **B2** in Scheme 1). The **B1** adduct can undergo a

* Corresponding author. E-mail: jrbarker@umich.edu.
[†] University of Michigan.
[‡] Università di Torino.

10.1021/jp077180k CCC: $40.75
Published on Web 03/18/2008

SCHEME 1: Reaction Mechanism for Ethyne + HO in the Presence of O_2

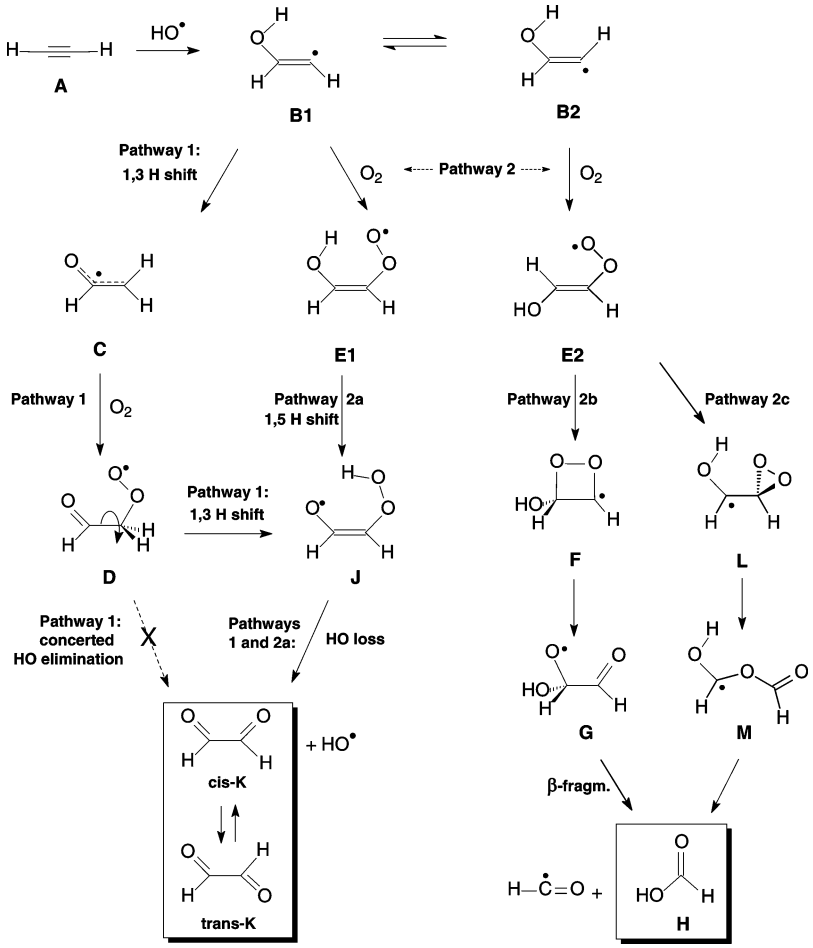

SCHEME 2: Ketene and CH_3 + CO Formation from C in the Reaction of Ethyne + HO in the Presence of O_2

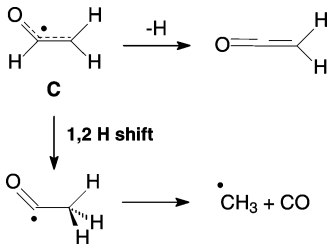

unimolecular 1,3 hydrogen shift to produce **C**, the vinoxyl radical, which has two resonance structures. **C** can decompose (Scheme 2), to form ketene + H, or isomerize, to form $OCCH_3$, which can subsequently decompose to produce CO + CH_3.[18,24] These two channels are relatively unimportant except at higher temperatures and low pressures. Ketene has been observed in photoionization experiments on the HO + C_2H_2 reaction in crossed effusive molecular beams (i.e., at very low pressures) in the absence of O_2.[11]

The two species produced by addition of HO to C_2H_2 (**B1** and **B2**) and their isomer **C** can react further with O_2 in bimolecular reactions to produce **E1**, **E2**, and **D**, respectively. Both species **E1** and **D** can undergo unimolecular hydrogen shift reactions to produce a common intermediate **J**. The weak O−O bond in **J** can break to produce *cis*- and *trans*-glyoxal (**K**) and HO radical. The oxygen-centered radical in intermediate **E2** can attack either end of the double bond to produce intermediates **F** and **L**. Intermediate **F**, which is a dioxetanyl free radical, reacts by breaking the O−O bond to produce **G**, which undergoes β-bond fission to produce formic acid (**H**) and formyl free radical. Intermediate **L**, which is a hydroxymethyl-substituted dioxiryl free radical, undergoes an unusual concerted reaction (see paper 1 for details) with a high barrier to produce **M**, which is relatively stable. However, **M** is produced with such a high vibrational excitation energy that it very rapidly undergoes C−O bond fission to give formic acid (**H**) and formyl free radical. Thus in the presence of O_2 the initial adducts (**B1** and **B2**) are converted to several products: glyoxal, formic acid, hydroxyl radical, and formyl free radical. Mechanisms are known for the subsequent atmospheric photo-oxidation of these product species.[1,25−27]

The reaction scheme for but-2-yne is analogous to that for ethyne, except that more reactions are possible (see Scheme 3; lowercase symbols are used for the but-2-yne mechanism). Thus the species produced in the presence of O_2 according to Scheme 3 include **o** (an enol derivative), **k2** (the keto form of biacetyl), **h** (acetic acid), acetyl free radical, and hydroxyl radical. In addition, we argue in paper 1 that RO_2 + $R'O_2$ reactions involving **e2** peroxyl radical can also produce glyoxal and HO_2 radical, as shown in Scheme 4. The biacetyl formed via this pathway is designated **k2**; below it is shown that biacetyl (designated **k1**) is also formed via another pathway. The oxidation of acetyl radicals has been considered recently by several groups,[23,28−30] and the atmospheric oxidation of most of the other organic species is moderately well understood.[1,25−27]

Background

As mentioned above, a number of studies have been reported on the temperature dependence and pressure falloff in the ethyne

SCHEME 3: Reaction Mechanism for But-2-yne + HO in the Presence of O_2• Reaction Channels Originating from e2

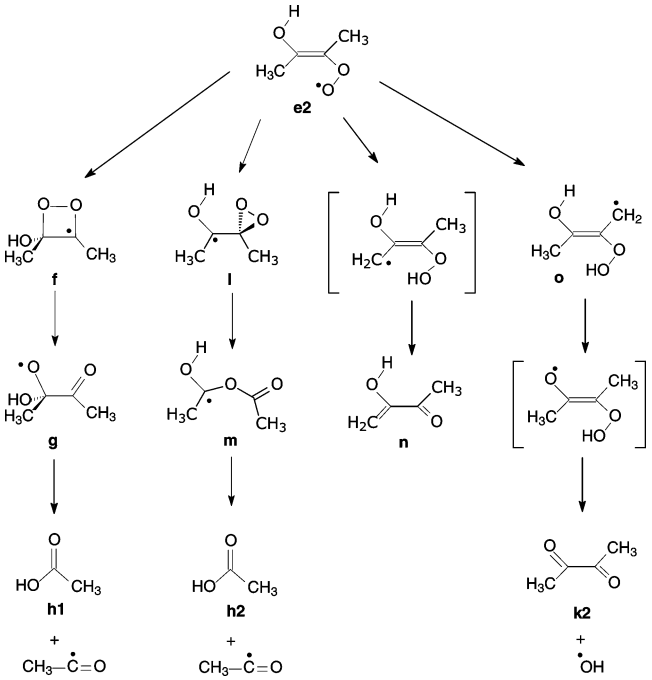

SCHEME 4: Glyoxal Formation from the Self-Reaction of Peroxyl Radical E2

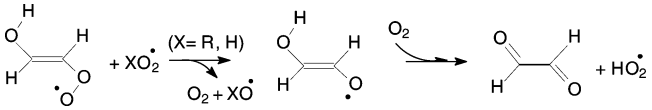

+ HO reaction system.[2−10] The two most recent studies[2,10] are the principal focus of the present work.

The pressure dependence of the reaction was studied by Sorensen et al. at 296 K in 25−750 Torr of air and O_2 buffer gases, by using relative rate techniques.[10] Their measurements ranged from 25 to 8000 Torr of synthetic air. They obtained the high-pressure limit rate constant $k_\infty = (9.69 \pm 0.30) \times 10^{-13}$ cm^3 molecule^{-1} s^{-1}, which is essentially identical to the current IUPAC recommended value 1.0×10^{-12} cm^3 molecule^{-1} s^{-1}.[31]

Very recently, McKee et al.[2] carried out a very careful study of the first step of the addition ethyne to HO in each of three vibrational states ($v = 0, 1, 2$). They used pressures of 50−760 Torr of N_2, He or SF_6, and measured rate constants by monitoring the hydroxyl radical decay with laser induced fluorescence. They analyzed the pressure falloff using Master Equation simulations to determine the Arrhenius parameters for the high-pressure limit rate constant, obtaining $A_\infty = (7.3 \pm 1.3) \times 10^{-12}$ cm^3 molecule^{-1} s^{-1} and $E_\infty = 5.3 \pm 0.4$ kJ mol^{-1}, which give $k_\infty = 8.6 \times 10^{-13}$ molecule^{-1} cm^3 s^{-1} at 298 K. Both their pressure falloff measurements and their k_∞ values are in good agreement with Sorensen et al.,[10] who used air as a collider instead of pure N_2. Both studies obtained values for k_∞ that are about half as large as those reported by Fulle et al.,[9] and concluded that the latter measurements are affected by unknown errors.

The first measurement of the products of the HO+C_2H_2 reaction was carried out by Kanofsky et al.[11] using photoionization mass spectrometry in crossed effusive molecular beams. The carrier gas (helium) pressures were very low and no O_2 was present. The only product detected had a mass corresponding to C_2H_2O (probably ketene).

Hatakeyama, Washida, and Akimoto (HWA)[14] measured the rate constants and the reaction mechanism of HO addition to ethyne in 1 atm of purified air at room temperature (they also investigated propyne and but-2-yne).[14] They monitored the products by FT-IR and found formic acid (40 ± 10%) and glyoxal (70 ± 30%) in the ethyne system, and acetic acid (12 ± 1%) and biacetyl (87 ± 7%) in the but-2-yne system. On the basis of the product analysis they suggested that the reaction passes through a peroxyl radical intermediate and that a four-member cyclic intermediate is responsible for the acid formation.

Formation of HO_2 from the reaction of HO with C_2H_2 in the presence of O_2 was demonstrated by Bohn et al.,[16,17] who suggested it was formed by the reaction HCO + O_2 → HO_2 + CO, consistent with the reaction mechanism proposed by HWA[14] and by Yeung, Pennino, Miller, and Elrod (YPME).[19]

Schmidt et al. reported that they detected vinoxyl radical in the C_2H_2 + HO reaction.[13] Many studies have been carried out to investigate the reactivity of vinoxyl radical. The results show that it mainly reacts with O_2 to form glyoxal and formaldehyde.[12,15,20] In all of these studies the vinoxyl radical was formed by photodissociation of methyl vinyl ether, or by H addition to ketene.[18]

There are few other studies of alkynes larger than ethyne. Boodaghians et al.[21] studied the rate and temperature dependence of the HO reaction with propyne, but-1-yne, but-2-yne, pent-1-yne, and hex-1-yne at low pressure. The order of reactivity they observed was propyne < 1-but-1-yne < 1-pent-1-yne < 1-hex-1-yne < 2-but-1-yne. YPME[19] carried out experiments at 100 Torr and 298 K in a turbulent flow reactor and detected the products by chemical ionization mass spectroscopy. Their measured yields of biacetyl and the acetic acid were 86 ± 11%, and 14 ± 11%, respectively, which are in very good agreement with the measurements of HWA.[14] They also calculated geometries and energies by using a variation of the G2 method,[32] but considered only the stable reactants, products and intermediates; transition state structures were not included. On the basis of the greater stability of the intermediate **L** compared to that of **F**, they suggested that the minimum energy pathway leading to the acid passes through **L**. In the present work, we extend the work of YPME by including transition state structures and additional reaction channels not previously taken into account.

Recently Senosiain, Klippenstein, Miller (SKM)[24] carried out a detailed theoretical study of the HO + C_2H_2 system by using ab initio electronic structure calculations and master equation simulations for a wide range of pressures and temperatures, with an emphasis on combustion conditions. However, they confined their attention to combustion conditions and to the C_2H_3O potential energy surface without including O_2 addition. Because they were dealing with fewer electrons than in the present study, they were able to carry out ab initio calculations at higher levels of theory. They obtained very good agreement with the existing laboratory data over very wide ranges of temperature and pressure.

Our aim is to understand the oxidation of alkynes in the atmosphere. In the present work, we have investigated the two simplest symmetric alkynes (ethyne and but-2-yne) in the presence of O_2, which adds considerable complexity. We expect that the mechanism obtained in the present work can be generalized to other alkynes, but larger and asymmetric alkynes have mechanisms that are even more complicated. Work is now underway on the mechanisms involving the asymmetric alkynes (propyne, but-1-yne, etc.).

Methods

Energy-dependent rate constants and product yields were calculated by using the MultiWell Program Suite.[33,34] According to the Rice−Ramsperger−Kassell−Marcus (RRKM) theory, the energy-dependent rate constant for a unimolecular reaction is written[35−38]

$$k(E) = \left[\frac{m^{\neq}\sigma}{m\sigma^{\neq}}\right]\frac{g_e^{\neq}}{g_e}\frac{1}{h}\frac{G^{\neq}(E - E_0^T)}{\rho(E)} \quad (1)$$

where the pairs of parameters m and $m^{\neq}$, σ and $\sigma^{\neq}$, and g_e and $g_e^{\neq}$, are the numbers of optical isomers, the external rotation symmetry numbers, and the electronic degeneracies for the reactant and transition state, respectively. $G^{\neq}(E - E_0^T)$ is the sum of states of the transition state and $\rho(E)$ is the density of states of the reactant; E_0^T is the critical energy for reaction, including zero-point-energy and centrifugal corrections at temperature T.

Following Forst,[37] the reactant and transition state were approximated as symmetric tops with principal moments of inertia $I_a \approx I_b$, I_c. By combining the two moments that are most similar to each other, one obtains the moment of inertia for a 2-dimensional (2-D) rotation ($I_{2D} = [I_aI_b]^{1/2}$). Because of conservation of angular momentum, the 2-D rotation is assumed to be inactive and is not used in calculating the sums and densities of states. The remaining one-dimensional degree of freedom (the K-rotor) is assumed to be active and constrained only by conservation of energy; it was used explicitly in the density of states calculations. Centrifugal corrections to the reaction thresholds were made by assuming the usual pseudo-diatomic model:[37]

$$E_0^T = E_0 - k_BT\left(1 - \frac{I_{2D}}{I_{2D}^{\neq}}\right) \quad (2)$$

where k_B is the Boltzmann constant, T is the temperature, I_{2D} and $I_{2D}^{\neq}$ are the 2D moments of inertia of reactant and transition state, respectively, and E_0 and E_0^T are the reaction critical energy for no rotation and after centrifugal corrections, respectively.

Corrections for quantum mechanical tunneling were included for all hydrogen transfer reactions by incorporating the corrections[39] for one-dimensional tunneling through an unsymmetrical Eckart barrier.[40]

The microcanonical unimolecular reaction rate constants can also be treated semi-empirically by using the Inverse Laplace Transform (ILT) method,[37,41,42] fitted to the experimental high-pressure rate constant:

$$k(E) = A_\infty\frac{\rho(E - E_\infty)}{\rho(E)} \quad (3)$$

where A_∞ and E_∞ are the Arrhenius parameters for the corresponding high-pressure limiting thermal rate constant. The reaction path degeneracy and centrifugal effects are included in A_∞. For added accuracy near the reaction threshold, E_∞ can be replaced in eq 3 by E_0, the reaction critical energy. This substitution tends to improve the threshold behavior, but at the cost of a small error in the calculated high-pressure limit activation energy.

Bimolecular reactions between excited species and O_2, which is present in great excess, may be important in some circumstances.[43] In the present work, these reactions were treated using the semi-microcanonical pseudo-first-order approach described recently.[23] The microcanonical bimolecular rate constant $k_{bim}(E)$ is given by an expression formally identical to eq 1, but where g_e, m, and σ are the products of the electronic degeneracies, the numbers of optical isomers, and the external symmetry numbers, respectively, of the two reactants. Furthermore, $\rho(E)$ is the convolution of rovibrational states of the two reactants, including the 2D external rotation (which is assumed to be active in the present treatment). Thermal distributions were assumed for relative translation and for the rotations of the two reactants. No centrifugal corrections were applied in calculating $k_{bim}(E)$.

Sums and densities of states were computed using the Beyer−Swinehart[44] and Stein−Rabinovitch[45] algorithms with an energy grain of $\Delta E_{grain} = 5$ cm^{-1}. This small grain size was used because it leads to more accurate microcanonical bimolecular reaction rate constants.[23] Densities and sums of states are stored by MultiWell in double arrays.[33] All of the elements in a double array are calculated using the same ΔE_{grain}; in the lower energy portion of the array, the sums and densities are tabulated for every energy grain, whereas in the upper part of the double array the values are tabulated with much larger energy spacing. In the present work, the lower part of the array consisted of 1500 array elements which ranged in energy from 0 to 7495 cm^{-1} (where the fluctuations in the density of states between adjacent energy grains is less than 5%). The higher energy part of the double array consisted of 500 elements ranging in energy from 0 to 60000 cm^{-1} with an energy spacing of 120.2 cm^{-1}.

Energy transfer was treated by assuming the exponential-down model for collision step-size distributions:

$$P(E,E') = \frac{1}{N(E')}\exp\left(-\frac{E' - E}{\alpha(E')}\right) \quad \text{for} \quad E' \geq E \quad (4)$$

where $P(E,E')$ is the probability of deactivation transitions from higher energy E' to energy E, $N(E')$ is a normalization factor, and the energy transfer parameter $\alpha(E')$ is approximately equal to the average energy transferred in deactivation collisions, $\langle\Delta E\rangle_{down}$. As described elsewhere,[46] $\alpha(E')$ is approximately a linear function of energy, and energy transfer experiments have shown it to be approximately independent of temperature, although in some chemical systems there is indirect evidence that it may be approximately proportional to temperature.[47] These conclusions depend at least in part on whether just vibrational energy is being considered in a master equation treatment, or total energy. Because in general, none of these dependences is known, the usual approach is to minimize the number of unfixed parameters by neglecting the energy dependence and by assuming either that there is no temperature dependence or that the temperature dependence is linear. In the present work, we have assumed that $\alpha(E')$ is independent of energy and that it is directly proportional to temperature. Furthermore, we have assumed that α is the same for all chemical species ("wells") in the master equation simulations and we have used α as an adjustable parameter to fit the limited experimental data available for the alkynes.

MultiWell is based on Gillespie's Stochastic Simulation Algorithm,[48,49] which is exact in the limit of an infinite number of stochastic trials.[50] For smaller numbers of trials, N_{trials}, the standard deviation σ_i in the population f_i of species i is given by the formula:[33]

$$\sigma_i = \sqrt{\frac{f_i(1 - f_i)}{N_{trials}}} \quad (5)$$

TABLE 1: Estimated Critical Properties and Lennard-Jones Parameters

	C_2HO_3 (B1)	C_4HO_7 (b1)	N_2 (ref 64)
	Critical Properties		
P_c (atm)	69	46	
V_c (cm^3 mol^{-1})	138	252	
T_c (K)	509	561	
	Lennard-Jones Parameters		
σ (Å)	4.10	5.00	3.74
ϵ/k_B (K)	455	489	82

In the present work, the number of stochastic trials was set to 10^6, which ensured relative errors below ~0.5% even for the lowest yields of present interest.

The Lennard-Jones parameters necessary for the collision frequency calculation were obtained from the literature or were estimated from critical properties by using the Miller, Lydersen and Vetere formulas for the critical temperature, critical pressure and critical volume, respectively.[51] Lennard-Jones parameters for the intermediates in the respective reaction systems were assumed to be the same as those estimated for the adducts (**B1** and **b1**) initially formed in the two systems. The estimated critical properties and Lennard-Jones parameters are given in Table 1.

In all of the following, the reaction yields are expressed relative to the net amount of alkyne consumed in a simulation. The simulations often show back-reaction that re-forms the original reactants. This effect is not observable in the yield experiments and so the results reported in the tables in this paper have been corrected for this effect. Back-reaction occurs at high temperature and low pressure, and is manifested by, for example, pressure falloff. At the high-pressure limit, back-reaction is negligible, but at low pressures it is quite significant. Original output from the simulations (not corrected for back-reaction) are reported in the Supporting Information.

Results and Discussion

Ethyne + HO Reaction. Simulations were initiated by assuming a chemical activation energy distribution[33] of **B1** produced by the C_2H_2 + HO reaction. Temperature (297 K), total pressure (760 Torr), buffer gas (N_2), and O_2 concentration (5.2×10^{18} molecules cm^{-3}) were chosen to reproduce the experimental conditions used by HWA.[14]

Although the results of Sorensen et al.,[10] who used synthetic air for the buffer gas, are as much as 25% higher than those obtained by McKee et al.[2] in pure N_2 buffer gas, the results are very similar and show similar experimental scatter (Figure 1). Therefore we assumed that N_2 and O_2 have identical energy transfer parameters. Figure 1 shows the experimental pressure-dependent rate constants and simulations carried out using three choices for the energy transfer parameter. The value $\alpha = 250$ cm^{-1}, used in most our simulations, is the best fit of to the data of McKee et al. The lower pressure data of Sorensen et al. could not be fitted very well, when even using very large values of α.

The density functional theory (DFT) calculations reported in paper 1 are expected to be accurate enough. However, DFT is known to be less accurate than other composite methods: Curtiss et al., comparing experimental and DFT enthalpies of formation of a set of molecules, found an average absolute error at DFT-(B3LYP) level, of about ±3 kcal mol^{-1}.[52] At 300 K, an error as small as 1 kcal mol^{-1} can change the rate constant by a factor 5. Thus we carried out simulations to investigate the effects of changing several critical reaction barriers. For example, simulations were carried out with the barriers calculated at the DFT level of theory without any corrections, with the **A**−**B1** barrier modified to fit the experimental k_∞, and with the modified **A**−**B1** barrier *and* the **B1**−**E1** and **B2**−**E2** barriers modified to fit generic experimental rate constants for Radical + O_2 recombination reactions (see refs 31 and 53). Furthermore, changes in the **E2**−**F** and **E2**−**L** energy barriers were made to test the sensitivity of the formic acid and glyoxal yields to these two parameters. Product yields resulting from these simulations, calculated with respect the consumed C_2H_2, are given in Table 2. The yields calculated with respect to the initially formed alkyne−O_2 adduct (some of which back-dissociates to regenerate the reactant alkyne) are given in the Supporting Information.

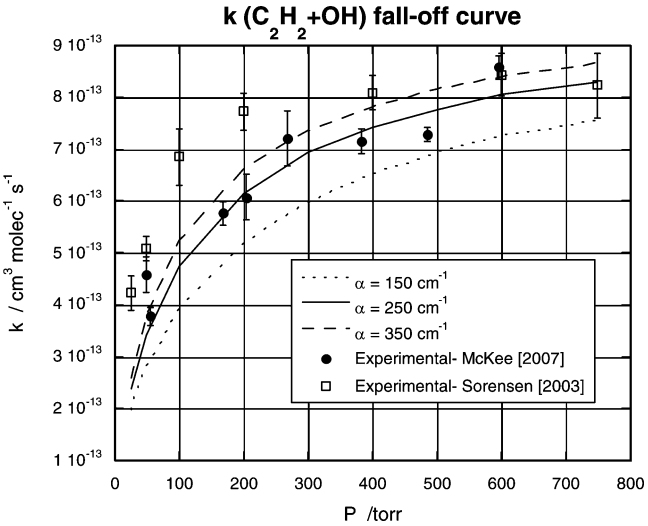

Figure 1. C_2H_2 + HO falloff curve (in N_2) and energy transfer parameters.

As discussed in paper 1, SKM[24] used a very high level of theory (RQCISD(T)/CBS) to predict accurate rate constants. Their energy barriers were calculated by using the CBS-QCI/APNO method, which is known to give very accurate energies. Their predicted rate constants are in very good agreement with the measurements reported by McKee et al.[2] Although such methods are more accurate than the DFT methods used in the present work, they are not feasible for systems with large numbers of electrons, as in the ethyne + HO + O_2 or but-2-yne reaction system. Furthermore, we have chosen to take some reaction parameters from other work and to adjust certain critical energy barriers, when appropriate. This pragmatic approach gives good results, as shown below.

The **A**−**B1** barrier was calculated by DFT to be −2.3 kcal mol^{-1}, relative to the separated reactants (all the reported barriers include the zero point energy corrections). The barrier height is negative because of the existence in the entrance channel of a van der Waals (vdW) complex with an even lower energy (−2.7 kcal mol^{-1}). In the present work, vdW complexes are neglected, as discussed below. However, the transition structure can be used with canonical transition state theory (TST) to calculate a rate constant (using Thermo, one of the codes included in the MultiWell Program Suite[33,34]). This was done by using harmonic oscillators or rigid free rotors for all degrees of freedom, except for the torsion, which was treated approximately[54] as a 2-fold hindered internal rotation with symmetry number of unity. To obtain a high-pressure limit rate constant in agreement with the IUPAC recommendation,[55] we used a **A**−**B1** barrier height of +1.7 kcal mol^{-1}, relative to reactants. Although this approach gives the correct rate constant at 298 K, the rate constant predicted at 800 K (8.4×10^{-12} molecule^{-1} cm^3 s^{-1}) and the predicted Arrhenius *A*-factor (A_∞

TABLE 2: Product Yields (Percent) for the C_2H_2 + HO Reaction in the Presence of O_2 from Simulations[a]

	note	α (cm^{-1})	**H1** (HCOOH via **F**)	**H2** (HCOOH via **L**)	total **H** (HCOOH)	**K** (glyoxal)	**E2**	total **E2** + glyoxal	ketene	CH_3 + CO
I	*b*	500	7.7	25.0	32.7	55.6	7.5	63.1	3.4	0.8
II	*b*	200	12.3	28.5	40.8	50.0	0.3	50.3	7.3	1.7
III	*c*	250	12.5	32.0	44.5	53.2	0.3	53.5	1.5	0.5
IV	*c,d*	250	12.6	34.4	46.6	51.8	0.3	52.2	1.0	0.3
V	*c,e*	250	12.4	29.8	42.2	54.0	0.2	54.2	2.8	0.8
VI	*c,f*	250	17.9	26.8	44.7	53.1	0.2	53.3	1.5	0.5
VII	*c,g*	250	10.2	34.6	44.8	53.1	0.1	53.2	1.5	0.5
VIII	*c,h*	250	12.4	30.5	42.9	50.7	0.0	50.7	5.0	1.4
XI	*c,i*	250	12.5	33.7	46.2	51.3	0.4	51.7	1.6	0.5
exp	*j*				40 ± 10			70 ± 30		

[a] T = 298K, P = 1 atm, buffer gas = N_2, $O_2 = 5.19 \times 10^{18}$ molecules cm^{-3}. Error bars ≤0.05%. [b] DFT energy barriers without adjustments. [c] Using the Arrhenius parameters calculated by McKee et al., and the energies calculated by SKM.[24] [d] T = 210 K. [e] T = 413 K. [f] Energy barrier **E2**−**F** decreased by 2 kcal mol^{-1}. [g] Energy barrier **E2**−**L** decreased by 2 kcal mol^{-1}. [h] $P(N_2)$ = 200 Torr, $O_2 = 1.36 \times 10^{18}$ molecules cm^{-3}. [i] Energy barriers **E1**−**B1** and **B2**−**E2** changed to fit the experimental rate constant. [j] See ref 14.

$= 2.0 \times 10^{-11}$ cm^3 $molecule^{-1}$ s^{-1}) are both almost three times as large as reported by McKee et al.,[2] who carried out the most recent and exhaustive study of the C_2H_2 + HO rate constant. For this reason we decided to model the C_2H_2 + HO rate constant by using the Inverse Laplace Transform[37,56,57] (ILT) semi-empirical approximation for the specific rate constant $k(E)$, parametrized with the Arrhenius parameters reported by McKee et al.

The high-pressure rate constants computed in the simulations using the ILT semi-empirical approximation for $k(E)$ agree exactly with those reported by McKee et al.[2] From the pressure-dependent data reported by McKee et al., we obtained the energy transfer parameter α for use in our master equation simulations. Following Miller and Klippenstein,[47] we assumed that α is proportional to temperature. The resulting simulations showed that the yields are almost independent of temperature in the range from 210 to 413 K (simulations IV and V in Table 2).

SKM[24] calculated molecular structures and energies for a number of species and reactions that are more important in combustion systems than in the atmosphere. We have incorporated some of their results in the present simulations. In particular, simulations III−IX were carried out using the vibrational frequencies and the energies calculated by SKM for **B1**, **B2**, **TS**−**B1**−**B2**, **TS**−**B**−**C**, **C**, and **TS**−**C**−ketene. The DFT frequencies and energies calculated in the present work were used for the remaining intermediates and transition structures. Some adjustments to the energies were made to fit experimental data.

In the present work, we lowered SKM's energy barrier for channel **B**−**C** by 2.3 kcal mol^{-1} (to 32.7 kcal mol^{-1}) to fit the experimental rate constant at the zero-pressure limit reported by Schmidt et al.:[13] 5×10^{-14} $molecule^{-1}$ cm^3 s^{-1}. This rate constant at the zero-pressure limit is somewhat lower than the one calculated by SKM[24] (8.8×10^{-14} $molecule^{-1}$ cm^3 s^{-1}) and is significantly lower than the one measured by Michael et al.[4] ($\sim 4 \times 10^{-13}$ $molecule^{-1}$ cm^3 s^{-1}). In the temperature range 228−413 K, the higher pressure measurements of Michael et al. and McKee et al.[2] are fairly consistent, but below 500 Torr the rate constants measured by Michael et al. in argon are up to ∼50% larger than those measured by McKee et al. in nitrogen. The fact that Michael et al. used Ar buffer gas and McKee et al. used N_2 is probably not the explanation for this discrepancy; in most systems, the N_2 collision efficiency is only 10%−30% larger than that for Ar.[46,58−60] There is generally good agreement among the high-pressure limit rate constants measured at 298 K: 8.3×10^{-13} $molecule^{-1}$ cm^3 s^{-1} (Schmidt et al.[13]), 9.7×10^{-13} $molecule^{-1}$ cm^3 s^{-1} (Sorensen et al.[10]), 8.6×10^{-13} $molec^{-1}$ cm^3 s^{-1} (McKee et al.[2]), 7.8×10^{-13} $molecule^{-1}$ cm^3 s^{-1} (Michael et al.[4]). Because the lower pressure data of Schmidt et al.[13] extend to very low pressures and also appear to be reasonably consistent with those of McKee et al.,[2] we chose to fit the zero-pressure rate constant of Schmidt et al.

The yields calculated by using the DFT energies without any corrections (simulation II) and those calculated using calculated energies from SKM (simulation III) are in quite good agreement. The total glyoxal yield only increased from 50% (II) to 53% (III) and the total formic acid yield increased from 41% (II) to 45% (III). The variation in the formic acid yield is attributable to the **B**−**C** transition state which was about 6 kcal mol^{-1} higher in simulation III, resulting in a lower ketene yield and increased formic acid. The fact that the yields are relatively insensitive to whether the energies are obtained by using RQCISD(T)/CBS or DFT is encouraging, because it shows that DFT, which is useful for larger molecules but is less accurate, gives reasonable results.

The rate constants for the O_2 addition to the vinyl radicals **B1** and **B2** at the high-pressure limit were calculated using canonical Variational Transition State Theory (VTST), based on the maximum of the free energy along the reaction path as the O−C distance was varied (the geometries were optimized at each point; see paper 1 for details): $k^{\infty}_{B1-E1} = 2.4 \times 10^{-11}$ $molecule^{-1}$ cm^3 s^{-1}, and $k^{\infty}_{B2-E2} = 1.7 \times 10^{-11}$ $molecule^{-1}$ cm^3 s^{-1}, respectively. These results can be compared to the experimental rate constant for the reaction (without making any distinction between B1 and B2) measured by Zetzsch and coworkers at 195 Torr of Ar buffer gas: 4.2×10^{-12} $molecule^{-1}$ cm^3 s^{-1}.[16,61] We expect this result at 195 Torr to be far below the high-pressure limit. The VTST rate constants are in reasonable agreement with the high-pressure limit for a similar reaction, $C_2H_3 + O_2$, which several experimental and modeling studies agree has a rate constant of $\sim 1 \times 10^{-11}$ cm^3 $molecule^{-1}$ s^{-1} at 300 K.[62] In the following, we use the VTST rate constants for most of the simulations, but in simulation XI we changed the energy barriers **B1**−**E1** (by +0.55 kcal mol^{-1}) and **B2**−**E2** (by +0.35 kcal mol^{-1}) to fit the experimental rate constant[62] ($C_2H_3 + O_2$, $k = (1.0 \pm 0.2) \times 10^{-11}$, in Table 3 of ref 62). This change had only a very modest effect on the product yields (see simulations III and XI): the changes are <2% for formic acid and for glyoxal.

Figure 2 shows the simulated yields of several species as functions of time, including the back-dissociation that regenerates the reactants (see Methods section). Because of their very low yields, intermediates **D**, **L**, **M**, and **E2** are not shown. In simulations initialized by formation of **B1**, the fraction of **B1** quickly decreases from unity because of the very fast isomer-

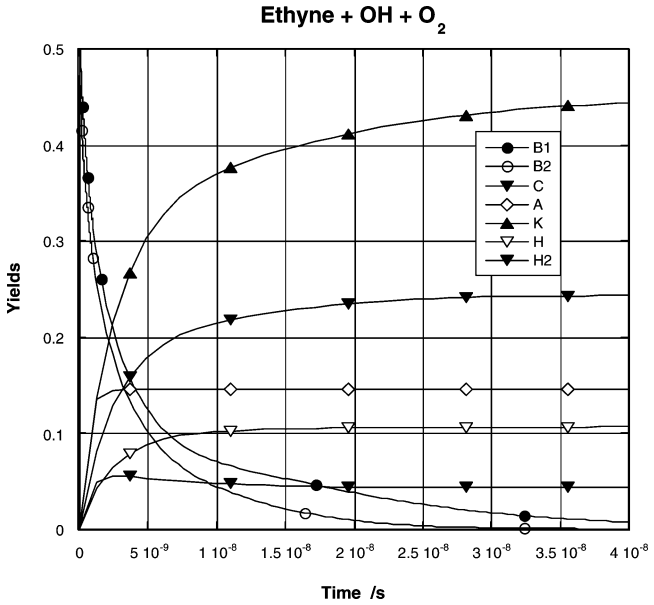

Figure 2. Simulated yields as function of the time. Simulation IV initiated by the chemical activation of **B1**, formed by C_2H_2 + HO (T = 297 K, P = 1 atm of N_2, α = 250 cm^{-1}).

ization and equilibration with **B2**. After only one collision at atmospheric pressure (~0.1 ns), the fraction of **B1** has dropped to 0.49 and that of **B2** is 0.44. The balance shows up as other products. The back-dissociation to produce **A** and the reactions leading to **C** are the channels with the highest energy barriers relative to **B1**, and therefore **A** and **C** can only be produced when **B1** is still highly vibrationally excited. After ~5 ns, **B1** has lost enough of its initial energy by thermalization with the collider gas so that **A** and **C** formation have ceased. According to the simulations, the yield of **K** is directly related to the loss of **B1**. Similarly, the yield of formic acid (**H**) is directly related to the loss of **B2**. Steady state is reached after about 50 ns at atmospheric pressure.

The calculated yields for the major species (with respect to C_2H_2 consumed) are listed in Table 2. The main factor affecting the yields is the energy transfer parameter α. To obtain an overview of the reaction yields, we first carried out a simulation using an arbitrary value: α = 500 cm^{-1} (simulation I), where α was assumed to be independent of energy, as discussed in the Methods section. For this simulation, the computed yield of formic acid (**H**) is much smaller than the experimental value. Moreover, the efficient collisional thermalization gives a larger **E2** yield. We hypothesized in paper 1 that the peroxyl radical **E2**, which is rather stable after thermalization (see Figure 3), can react in bimolecular reactions with itself (self-reaction) or with other peroxyl radicals (including HO_2) to produce more glyoxal (**K**), following the mechanism shown in Scheme 4 (see paper 1 for discussion). Reaction channel **E1**−**J** produces glyoxal in only the *cis* conformation, but the reactions in Scheme 4 produce only *trans*-glyoxal. However, the energy barrier for the *cis*−*trans* isomerization in glyoxal is so small (only about 1 kcal mol^{-1}) that the two isomers equilibrate very rapidly at room temperature. Due to the low concentrations of peroxyl radicals (RO_2 or HO_2) in the atmosphere and in laboratory experiments, bimolecular reactions involving **E2** are expected to be at least an order of magnitude slower than the competing unimolecular channels leading to glyoxal formation (**E1**−**J**) or to formic acid (**E2**−**L**−**M** and **E2**−**F**−**G**). Furthermore, bimolecular reactions will be most important only when **E2** is completely thermalized. For this reason, the bimolecular reaction

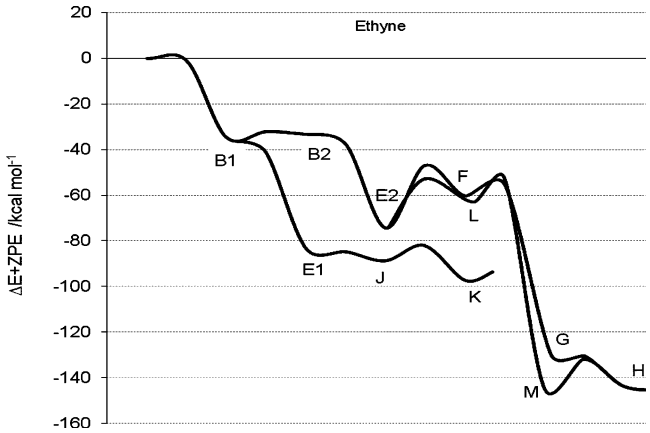

Figure 3. Potential energy profile (including zero point energies) of the main channels for reactions of HO with C_2H_2 in the presence of O_2. For definitions of the labels, see the reaction schemes.

channels involving **E2** were not included in our master equation simulations, but the total glyoxal yields in Tables 2 and 3 include the amount of thermalized **E2** produced in the simulations.

The experimental falloff curve can be fitted (see above) by reducing α to 200 cm^{-1} (simulation II). This also produces fortuitously exact agreement between the simulation and the experimental formic acid yield (41%).[14] In this simulation, the computed glyoxal yield (50%) differs from the experimental value[14] (70 ± 30%), but it is still within the experimental error bars.

Formic acid is formed via two separate paths, both of which originate from the **E2** peroxyl radical. About one-third of the total acid is formed via the path that passes through **F** and **G**, and the balance is produced via the path that passes through **L** and **M**. Species **L** and **F** fortuitously have similar energies, and therefore the two reaction paths are of roughly equal importance. The formic acid produced by these two paths is designated **H1** and **H2**, respectively, in Scheme 5. The total formic acid and glyoxal yields decrease at low pressure, but the ratio remains almost constant. The simulation (VIII) carried out at 200 Torr predicted **H1** = 12.4% and **H2** = 30.5%, but the **H2**/**H1** ratio is still ~2.5, which is about the same as at atmospheric pressure. The reduction of the product yields at lower pressure is due to the **B1**−**C** channel, which becomes more important under these conditions (see below).

The only difference between **H1** and **H2** is the origin of the carboxylic oxygen: in **H1**, the oxygen comes exclusively from the terminal peroxylic oxygen atom of **E2**, whereas in **H2** both peroxylic oxygen atoms have an equal chance to become carboxylic (see Scheme 5). There is no simple way to distinguish the two channels experimentally. By modifying the **E2**−**F** and **E2**−**L** energy barriers (simulations VI and VII, respectively), it is possible to observe a change in the ratio **H2**/**H1**, while the formic acid (~45%) and the glyoxal (~53%) yields remain almost constant. Decreasing the **E2**−**F** energy barrier by 2 kcal mol^{-1} causes the **H1** yield to increase and the **H2** yield to decrease by the same amount (simulation IX, compared to simulation III). The **H1** and **H2** yields are less sensitive to variations of the **E2**−**L** barrier (simulation VII).

Our simulations predict vinoxyl radical (**C**) formation, but **C** quickly dissociates completely via two channels to produce ketene + H and CH_3 + CO. A third possible channel, oxygen addition to form **D**, is negligible: the yield of **D** is <0.01%. At atmospheric pressure, products formed via **C** (i.e., ketene and CH_3 + CO) constitute about 7% of the total amount of C_2H_2 consumed. This yield is inconsistent with the upper limit of

TABLE 3: Product Yields (Percent) for the C_4H_6 + HO Reaction in the Presence of O_2 from Simulations[a]

	note	α (cm^{-1})	H via **f**	H via **l**	total **h**	**k1**	**k2**	**e2**	total **e2 + k1 + k2**	**n**	**c**
1	*b*	200	2.2	34.9	37.1	57.0	1.6	0.1	58.7	4.0	0.2
2	*b*	400	1.4	28.4	29.8	63.6	1.0	2.5	67.1	2.9	0.1
3	*b*	500	1.1	24.4	25.5	66.8	0.8	4.0	71.6	2.4	0.1
4	*c*	500	1.1	23.7	24.8	67.4	0.7	4.2	72.3	2.3	<0.1
5	*b*	600	1.0	20.7	21.7	69.6	0.6	5.1	75.3	2.1	0.1
6	*b*	700	0.8	17.7	18.5	71.8	0.6	6.0	78.4	1.9	0.1
7	*b*	900	0.7	13.2	13.9	75.0	0.2	7.5	82.6	1.4	<0.1
8	*d*	500	2.6	23.2	25.7	66.8	0.7	3.9	71.4	2.3	0.1
9	*e*	500	0.9	26.1	27.0	66.8	0.6	3.3	70.7	1.8	0.1
10	*f,h*	500	1.3	27.0	28.3	67.0	1.1	0.7	68.7	2.3	0.6
exp	*g*				12 ± 1				87 ± 7		
exp	*h*				14 ± 11				86 ± 11		

[a] T = 298K, P = 1 atm, buffer gas = N_2, O_2 = 5.19 × 10^{18} molecules cm^{-3}. Error bars ≤0.05%. [b] DFT energy barriers without adjustments. [c] Energy barrier C_4H_2 + HO changed to fit the experimental rate constant (see text). [d] Energy barrier **e2**−**f** decreased by 2 kcal mol^{-1}. [e] energy barrier **e2**−**l** decreased by 2 kcal mol^{-1}. [f] T = 298 K, P = 100 Torr N_2, [O_2] = 6.50 × 10^{17} molecules cm^{-3}. [g] See ref 14. [h] See ref 19.

SCHEME 5: Isotopic Differences between H1 and H2, Which Originate from E2 in the Reaction Ethyne + HO in the Presence of O_2

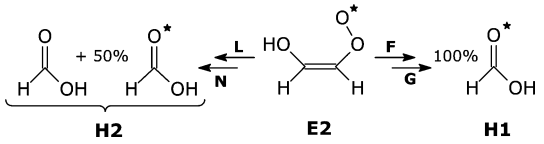

~0.5% reported by HWA.[14] The yield is overestimated when using energies calculated at the DFT level of theory (simulation II), because the DFT method underestimates of the **B**−**C** energy barrier. According to the present DFT results with no adjustments, the **B**−**C** transition structure is located 2.6 kcal mol^{-1} *below* the HO + C_2H_2 reactants. In contrast, SKM[63] and McKee et al.[2] used higher levels of theory and obtained energies of 3.9 and 2.6 kcal mol^{-1} *above* the reactants, respectively. As discussed above, we adjusted the **B**−**C** energy barrier to fit the zero pressure rate constant reported by Schmidt et al.[13] with the result that the transition state lies 1.6 *above* the reactants. With this value, the yield of **C** decreases to 1−3% (simulations III−VII), which is more consistent with the upper limit reported by HWA.[14] Note that the yield of **C** is pressure dependent, and at 200 Torr it increases to about 6.4%: at low pressure the number of collisions is lower, so thermalization takes place more slowly and there is more opportunity for **B1** to react and produce **C**.

But-2-yne + HO Reaction. In these simulations (Table 3), the sums and densities of states were calculated with an energy grain of 5 cm^{-1}. In the MultiWell double arrays, every energy grain is used from 0 to 1995 cm^{-1} in the lower part of the array, and energies from 0 to 60 000 cm^{-1} are used with ΔE_{grain} = 606.1 cm^{-1} spacing in upper part of the arrays. At 2000 cm^{-1}, the grain-to-grain fluctuations in the densities of states are less than 5%, suitable for accurate calculations using MultiWell. The energies obtained using DFT were used in the simulations without further adjustments.

The reaction mechanism of but-2-yne + HO is similar to that for ethyne + HO, but the presence of two methyl groups opens two new reaction channels involving peroxyl radical **e2** (Scheme 3). In addition to the ring closure to form either the dioxiranyl intermediate (channel **e2**−**l**) or the dioxetanyl intermediate (channel **e2**−**f**), the terminal peroxylic oxygen can also abstract a hydrogen from the methyl groups. Depending on which hydrogen is abstracted (from the *gem*-methyl or *trans*-methyl), it is possible to form biacetyl (channel **e2**−**o**−**k2**) or an α,β-unsaturated carbonyl compound (channel **e2**−**n**). In solution

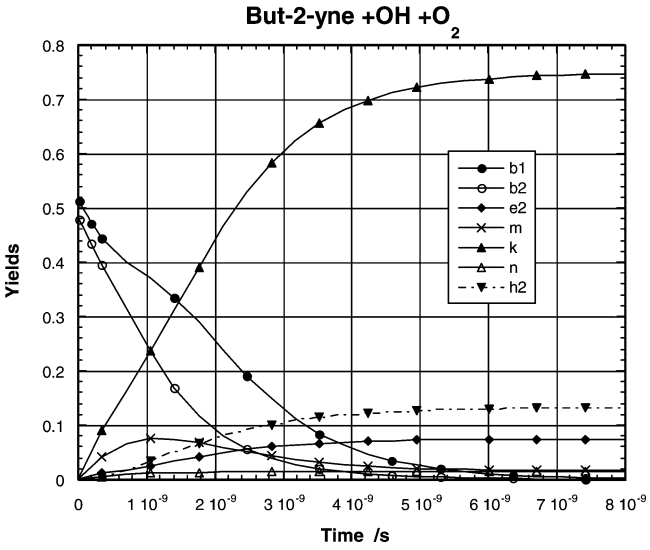

Figure 4. Simulated yields as function of the time. Simulation initiated by the chemical activation of **b1**, formed by C_4H_6 + HO (T = 297 K, P = 1 atm of N_2, α = 900 cm^{-1}).

phase or on surfaces, the enolic α,β-unsaturated carbonyl (**n**) may quickly interconvert by acid or base catalysis to the ketonic form (**k2**), but the barrier for the gas-phase unimolecular interconversion is too high (53.3 kcal mol^{-1}) for the reaction to be significant. In conclusion, the mechanism **e1**−**k1,** remains the main source of biacetyl (**k1**), and the other channels (**e2**−**n** and **e2**−**o**−**k2**) make smaller contributions. According to our simulations, the α,β-unsaturated carbonyl (**n**) constitutes a small but possibly measurable fraction (1−4%) of the total products, but HWA did not report detecting such compounds.[14]

Unfortunately only a very limited number of experiments have been carried out by using but-2-yne, and a falloff curve for the HO addition to C_4H_6 in N_2 buffer gas is not available. However, simulations arbitrarily using α = 200 cm^{-1} predict that the high-pressure rate limit is reached at very low pressure (~1 Torr), and the rate constant reaches 50% of the high-pressure limit at only ~10^{-4} Torr. Thus the reaction is effectively in the high-pressure limit at all pressures of tropospheric interest. It is reasonable to expect the α parameter for but-2-yne to be larger than that for ethyne, and so we chose to carry out simulations (Table 3) with a range of values from α = 200 cm^{-1} to α = 900 cm^{-1}, which we believe to be realistic for but-2-yne.

The time-dependent yields (for α = 500 cm^{-1}) are reported in Figure 4, where it is apparent that but-2-yne is predicted to react with HO faster than does ethyne. Steady state is reached

after only ~8 ns. There are some important differences between the but-2-yne + HO system and the C_2H_2 + HO system. Due to the higher densities of states of the intermediates in the but-2-yne + HO system, the intermediates have longer lifetimes and experience more efficient thermalization. Thus the fraction of the initially excited adduct that reacts by re-dissociation back to the reactants is completely negligible and the reaction is very near the high-pressure limit. In addition, intermediates **n** and **l** are collisionally stabilized, although in low concentration.

The experimental rate constant for addition of HO to C_4H_6 is 3.0×10^{-11} molecule^{-1} cm^3 s^{-1}.[14] From this value and by using the A-factor based on DFT-calculated frequencies and moments of inertia, the "experimental" barrier was estimated to be $E_a = -1.1$ kcal mol^{-1}. In many simulations, we assumed the barrier is 0.0 kcal mol^{-1}, with corresponding rate constant 5.7×10^{-12} molecule^{-1} cm^3 s^{-1}. Adjustment of the C_4H_6 + HO barrier (simulation 4, Table 3) to fit the experimental rate constant does not affect the yields significantly, compared with the DFT calculated barrier (simulation 3). Whether the calculated or experimental barrier is used, the acetic acid (**h**) yield changes by only 0.7% and the total biacetyl yield (sum of **e2**, **k1** and **k2**) increases by the same amount. As already found for ethyne, the energy barrier for the HO addition does not play a key role in determining the reaction yields.

Depending on the value of α, the total yield of formic acid varies from 13.9% ($\alpha = 900$ cm^{-1}, simulation 7) to 37.1% ($\alpha = 200$ cm^{-1}, simulation 1). The major source of acetic acid is the channel **e2**−**l**−**m**, and the second pathway (**e2**−**f**−**g**) is very minor. This result is quite unlike the ethyne system. This is because the but-2-yne system has a barrier for the **e2**−**f** reaction that is ~1 kcal mol^{-1} higher than the **E2**−**F** channel in the ethyne system, and (even more important) the **e2**−**l** barrier is 4 kcal mol^{-1} smaller than the **E2**−**L** barrier in the ethyne system. Because of these two factors, the **h2** yield is much larger than that of **h1**.

Energy transfer also affects other yields. The yield of biacetyl (**k2**) depends strongly on α. Total biacetyl is the sum of three different channels (but **b1**−**j** is dominant) and goes from the 58.7% for $\alpha = 200$ cm^{-1} (simulation 1) to 82.6% for $\alpha = 900$ cm^{-1} (simulation 7). The second unimolecular channel for the biacetyl formation (**e2**−**o**) contributes only ≤1.6%, because of the high reaction barrier (26.4 kcal mol^{-1}) and efficient thermalization. These effects also explain the relatively high yield of **e2**, especially when α is large. The bimolecular reactions of **e2** (Scheme 4) are predicted to yield up to 6% of biacetyl (this is the third channel).

In the simulations carried out using $\alpha = 400$ cm^{-1} (simulation 2), 500 cm^{-1} (simulation 3), 600 cm^{-1} (simulation 5), and 700 cm^{-1} (simulation 6), and 900 cm^{-1} (simulation 9) the acetic acid (**h**) yields decrease almost linearly, and biacetyl increases with the same trend. Simulation 9 ($\alpha = 900$ cm^{-1}) gives yields in perfect agreement with the measurements by HWA and YPME, but considering the experimental error bars, satisfactory agreement is also obtained using values as low as $\alpha = 500$ cm^{-1}. Simulation 1 (Table 3, $\alpha = 200$ cm^{-1}) can be compared directly with simulation II (Table 2): the carboxylic acid and the carbonyl yields are similar in the two cases, but the but-2-yne simulation (simulation 1, Table 3) does not agree with the experimental data.

Simulations carried out for YPME's experimental conditions[19] (simulation 10) and for HWA's conditions[14] (simulation 3), and with $\alpha = 500$ cm^{-1}, predicted essentially the same yields for both acetic acid and biacetyl. The **e2** yield from simulation 3 is larger than that from simulation 10, because the pressure in YPME's experiments is lower, and therefore **e2** can react to a greater extent before thermalization. Also, variations in the barriers for channel **e2**−**f** (simulation 8) and channel **e2**−**l** (simulation 9) were found to change the relative weight of the two channels to some extent, but the total acetic acid (**h**) and biacetyl (**k1** + **k1** + **e2**) yields remained almost constant. This is a strong indication that, at least for controlling the yields, the value of α is at least as important as the barrier heights.

The yield of **c** (3-oxobutyl radical) is always below 0.6%: much lower than that obtained from the ethyne simulations. This is because **b1** (in the but-2-yne mechanism) is thermalized by collisions more efficiently due to its higher density of states and longer lifetime with respect to isomerization reactions, regardless of the α value. The barrier **b1**−**c** is so high that **c** radical is produced only when the number of collisions is very small (at very low pressure).

Conclusions

Reaction mechanisms for ethyne + HO and but-2-yne + HO in the presence of O_2 were developed by using ab initio electronic structure calculations adjusted (for the ethyne mechanism) to fit existing data for reaction rates and yields. Multichannel, multiwell master equation simulations showed that two channels, **E2**−**L**−**M** and **E2**−**F**−**G**, contribute to formation of formic acid in the ethyne system, but only the first channel is important in the but-2-yne system. In the but-2-yne system, biacetyl **k** can be formed via the unimolecular channel **E1**−**J**, or by bimolecular reactions (see Scheme 4), but the latter channel is relevant only when the energy transfer is fast enough ($\alpha \geq 400$ cm^{-1}) or pressures are high enough to thermalize **E2** before unimolecular reactions can compete. In the but-2-yne system, the **e2**−**o** channel is possible but contributes <1% to the total biacetyl yield. The relative yields are quite insensitive to the energy barriers of alkyne + HO addition and **E2**−**F** and **E2**−**L** isomerization channels.

The energy transfer parameter (α) appears to be the most important for obtaining satisfactory yields in the master equation simulations. The results for ethyne, where pressure falloff data are available to help in estimating α, are in good agreement with the experimental yield data. Yield predictions in qualitative agreement with the scanty experimental data for the but-2-yne system were obtained by using a range of α values (400−900 cm^{-1}). Using lower values of α (e.g., $\alpha = 200$ cm^{-1}) gave unsatisfactory results.

Master equation simulations have proved to be reliable theoretical tools for studying rates and mechanisms. Along with potential energy surface and harmonic vibrational analysis, obtained by ab initio calculations, they allow qualitative or even quantitative predictions of yields and rates. However, the accuracy of the quantum chemistry calculations and the collision efficiency both play important roles. DFT energies are sufficient to obtain quite good yields, but a higher level of theory is needed for near-quantitative predictions. To improve the overall accuracy, small empirical adjustments to the calculated energy barriers can be made by fitting experimental rate constants. Energy transfer can usually be estimated only from experimental falloff curves, but yield ratios can also be used in some cases, as in the present work. A more extensive knowledge of the energy transfer processes is needed to make the master equation simulations quantitatively predictive. However, the semi-empirical models developed here are satisfactory for atmospheric chemistry applications.

Acknowledgment. Correspondence with Matthias Olzmann is gratefully acknowledged. This work was supported in part

by NSF (Atmospheric Chemistry Division), by NASA-Upper Atmosphere Research Program, and by NASA-Planetary Atmospheres.

Supporting Information Available: Optimized geometries, energies, harmonic vibrational frequencies and moments of inertia (K-rotor, and 2D-rotors). See also "Supporting Information" in paper 1. This material is available free of charge via the Internet at http://pubs.acs.org.

References and Notes

(1) Finlayson-Pitts, B. J.; Pitts, J. N., Jr. *Chemistry of the Upper and Lower Atmosphere*; Academic Press: San Diego, 2000.
(2) McKee, K. W.; Blitz, M. A.; Cleary, P. A.; Glowacki, D. R.; Pilling, M. J.; Seakins, P. W.; Wang, L. *J. Phys. Chem. A* **2007**, *111*, 4043−4055.
(3) Perry, R. A.; Atkinson, R.; Pitts, J. N. *J. Chem. Phys.* **1977**, *67*, 5577−5584.
(4) Michael, J. V.; Nava, D. F.; Borkowski, R. P.; Payne, W. A.; Stief, L. J. *J. Chem. Phys.* **1980**, *73*, 6108−6116.
(5) Perry, R. A.; Williamson, D. *Chem. Phys. Lett.* **1982**, *93*, 331−334.
(6) Smith, G. P.; Fairchild, P. W.; Crosley, D. R. *J. Chem. Phys.* **1984**, *81*, 2667−2677.
(7) Liu, A. D.; Mulac, W. A.; Jonah, C. D. *J. Phys. Chem.* **1988**, *92*, 5942−5945.
(8) Lai, L. H.; Hsu, Y. C.; Lee, Y. P. *J. Chem. Phys.* **1992**, *97*, 3092−3099.
(9) Fulle, D.; Hamann, H. F.; Hippler, H.; Jansch, C. P. *Ber. Bunsen-Ges. Phys. Chem.* **1997**, *110*, 1433−1442.
(10) Sorensen, M.; Kaiser, E. W.; Hurley, M. D.; Wallington, T. J.; Nielsen, O. J. *Int. J. Chem. Kinet.* **2003**, *35*, 191−197.
(11) Kanofsky, J. R.; Lucas, D.; Pruss, F.; Gutman, D. *J. Phys. Chem.* **1974**, *78*, 311−316.
(12) Gutman, D.; Nelson, H. H. *J. Phys. Chem.* **1983**, *87*, 3902−3905.
(13) Schmidt, V.; Zhu, G. Y.; Becker, K. H.; Fink, E. H. *Ber. Bunsen-Ges. Phys. Chem. Chem. Phys.* **1985**, *89*, 321−322.
(14) Hatakeyama, S.; Washida, N.; Akimoto, H. *J. Phys. Chem.* **1986**, *90*, 173−178.
(15) Zhu, L.; Johnston, G. *J. Phys. Chem.* **1995**, *99*, 15114−15119.
(16) Bohn, B.; Siese, M.; Zetzsch, C. *J. Chem. Soc., Faraday Trans.* **1996**, *92*, 1459−1466.
(17) Bohn, B.; Zetzsch, C. *J. Chem. Soc., Faraday Trans.* **1998**, *94*, 1203−1210.
(18) Lee, J.; Bozzelli, J. W. *Int. J. Chem. Kinet.* **2003**, *35*, 20−44.
(19) Yeung, L. Y.; Pennino, M. J.; Miller, A. M.; Elrod, M. J. *J. Phys. Chem. A* **2005**, *109*, 1879−1889.
(20) Delbos, E.; Fittschen, C.; Hippler, H.; Krasteva, N.; Olzmann, M.; Viskolcz, B. *J. Phys. Chem. A* **2006**, *110*, 3238−3245.
(21) Boodaghians, R. B.; Hall, I. W.; Toby, F. S.; Wayne, R. P. *J. Chem. Soc., Faraday Trans. 2* **1987**, *83*, 2073−2080.
(22) Maranzana, A.; Ghigo, G.; Tonachini, G.; Barker, J. R. *J. Phys. Chem. A* **2008**, *112*, 3656−3665.
(23) Maranzana, A.; Barker, J. R.; Tonachini, G. *Phys. Chem. Chem. Phys.* **2007**, *9*, 4129−4141.
(24) Senosiain, J. P.; Klippenstein, S. J.; Miller, J. A. *J. Phys. Chem. A* **2005**, *109*, 6045−6055.
(25) Atkinson, R. *Atmos. Environ.* **2000**, *34*, 2063−2101.
(26) Atkinson, R.; Arey, J. *Chem. Rev.* **2003**, *103*, 4605−4638.
(27) Seinfeld, J. H.; Pandis, S. N. *Atmospheric Chemistry and Physics*; John Wiley & Sons: New York, 1998.
(28) Blitz, M. A.; Heard, D. E.; Pilling, M. J. *Chem. Phys. Lett.* **2002**, *365*, 374−379.
(29) Kovacs, M. A.; Javan, A. *J. Chem. Phys.* **1969**, *50*, 4111−4112.
(30) Talukdar, R. K.; Davis, M. E.; Zhu, L.; Ravishankara, A. R.; Burkholder, J. B. "Determination of the OH Radical Yield in the $CH_3CO + O_2$ Reaction"; 19th International Symposium on Gas Kinetics, 2006, Orleans, France.
(31) Atkinson, R.; Baulch, D. L.; Cox, R. A.; Crowley, J. N.; Hampson, R. F.; Hynes, R. G.; Jenkin, M. E.; Rossi, M. J.; Troe, J. *Atmos. Chem. Phys.* **2006**, *6*, 3625−4055.
(32) Curtiss, L. A.; Raghavachari, K.; Trucks, G. W.; Pople, J. A. *J. Chem. Phys.* **1991**, *94*, 7221−7230.
(33) Barker, J. R. *Int. J. Chem. Kinet.* **2001**, *33*, 232−245.
(34) Barker, J. R.; Ortiz, N. F.; Preses, J. M.; Lohr, L. L.; Maranzana, A.; Stimac, P. J. "MultiWell-2.08 Software," (Development Version) 2007.
(35) Baer, T.; Hase, W. L. *Unimolecular Reaction Dynamics. Theory and Experiments*; Oxford University Press: New York, 1996.
(36) Gilbert, R. G.; Smith, S. C. *Theory of Unimolecular and Recombination Reactions*; Blackwell Scientific: Oxford, U.K., 1990.
(37) Forst, W. *Theory of Unimolecular Reactions*; Academic Press: New York, 1973.
(38) Robinson, P. J.; Holbrook, K. A. *Unimolecular Reactions*; Wiley-Interscience: New York, 1972.
(39) Miller, W. H. *J. Am. Chem. Soc.* **1979**, *101*, 6810−6814.
(40) Eckart, C. *Phys. Rev.* **1930**, *35*, 1303−1309.
(41) Forst, W. *J. Phys. Chem.* **1983**, *83*, 100−108.
(42) Forst, W. *Unimolecular Reactions. A Concise Introduction*; Cambridge University Press: Cambridge, U.K., 2003.
(43) Olzmann, M. *Phys. Chem. Chem. Phys.* **2002**, *4*, 3614−3618.
(44) Beyer, T.; Swinehart, D. F. *Commun. Assoc. Comput. Machines* **1973**, *16*, 379.
(45) Stein, S. E.; Rabinovitch, B. S. *J. Chem. Phys.* **1973**, *58*, 2438−2445.
(46) Barker, J. R.; Yoder, L. M.; King, K. D. *J. Phys. Chem. A* **2001**, *105*, 796−809.
(47) Miller, J. A.; Klippenstein, S. J. *Phys. Chem. Chem. Phys.* **2004**, *6*, 1192−1202.
(48) Gillespie, D. T. *J. Comput. Phys.* **1976**, *22*, 403−434.
(49) Gillespie, D. T. *J. Phys. Chem.* **1977**, *81*, 2340−2361.
(50) Gillespie, D. T. *Physica A (Amsterdam)* **1992**, *188*, 404−425.
(51) *Perry's Chemical Engineer's Handbook*, 6th ed.; Green, D. W., Maloney, J. O., Eds.; McGraw-Hill, Inc.: New York, 1984.
(52) Curtiss, L. A.; Raghavachari, K.; Redfern, P. C.; Pople, J. A. *J. Chem. Phys.* **1997**, *106*, 1063−1079.
(53) Sander, S. P.; Friedl, R. R.; Ravishankara, A. R.; Golden, D. M.; Kolb, C. E.; Kurylo, M. J.; Molina, M. J.; Moortgat, G. K.; J. Finlayson-Pitts, B.; Wine, P. H.; Huie, R. E.; Orkin, V. L. Chemical Kinetics and Photochemical Data for Use in Stratospheric Modeling. Evaluation Number 15; Jet Propulsion Laboratory: Pasadena, CA, 2006, http://jpldataeval.jpl-.nasa.gov/.
(54) Barker, J. R.; Shovlin, C. N. *Chem. Phys. Lett.* **2004**, *383*, 203−207.
(55) Atkinson, R.; Cox, R. A.; Crowley, J.; Hampson, R. F.; Hynes, R. G.; Jenkin, M. E.; Kerr, J. A.; Rossi, M. J.; Troe, J. Summary of Evaluated Kinetic and Photochemical Data for Atmospheric Chemistry. Section II - Organic Reactions; IUPAC Subcommittee for Gas Kinetic Data Evaluation for Atmospheric Chemistry: Cambridge, U.K., 2006, http://www.iupac-kinetic.ch.cam.ac.uk/index.html.
(56) Forst, W. *J. Phys. Chem.* **1972**, *76*, 342−348.
(57) Slater, N. B. *Theory of Unimolecular Reactions*; Cornell University Press: Ithaca, NY, 1959.
(58) Tardy, D. C.; Rabinovitch, B. S. *Chem. Rev.* **1977**, *77*, 369−408.
(59) Oref, I.; Tardy, D. C. *Chem. Rev.* **1990**, *90*, 1407−1445.
(60) Hippler, H.; Troe, J. Recent direct studies of collisional energy transfer on vibrationally excited molecules in the electronic ground state. In *Advances in Gas-Phase Photochemistry and Kinetics: Bimolecular Collisions*; Ashfold, M. N. R., Baggott, J. E., Eds.; The Royal Society of Chemistry: London, 1989; pp 209.
(61) Siese, M.; Zetzsch, C. *Z. Phys. Chem.-Int.* **1995**, *199*, Part 1, 75−89.
(62) Laufer, A. H.; Fahr, A. *Chem. Rev.* **2004**, *104*, 2813−2832.
(63) Senosiain, J. P.; Klippenstein, S. J.; Miller, J. A. *J. Phys. Chem. A* **2006**, *110*, 6960−6970.
(64) Hippler, H.; Troe, J.; Wendelken, H. J. *J. Chem. Phys.* **1983**, *78*, 6709−6717.